Wear 306 (2013) 263–275

Contents lists available at ScienceDirect

Wear

journal homepage: www.elsevier.com/locate/wear

The chemical wear (corrosion-wear) of novel Cr based hard coated 316L austenitic stainless steels in aqueous saline solution

P.A. Dearnley [a,*], B. Mallia [b]

[a] nCATS, Engineering Sciences, University of Southampton, Southampton SO17 1BJ, UK
[b] University of Malta, Msida MSD 2080, Malta

ARTICLE INFO

Article history:
Received 3 June 2012
Received in revised form
19 July 2012
Accepted 17 September 2012
Available online 8 October 2012

Keywords:
Tribo-corrosion
Surface engineering
Corrosion-wear

ABSTRACT

Austenitic stainless steels are prone to galling and seizure in sliding contacts and display poor resistance to corrosion-wear. The purpose of this paper was to discover if the surface engineering of austenitic stainless steel via the application of Cr based hard coatings can alleviate this problem. Corrosion-wear tests using an aluminium oxide ball (pin) to slide against coated and uncoated AISI 316L in 0.9% NaCl solution under a normal force ~1 N revealed degradation, under open circuit potential conditions, to be dominated by mechanically antagonized corrosion (Type I corrosion-wear) for all the test materials. A minor contribution to degradation was caused through superficial plastic deformation (micro-asperity shearing) of the contact surfaces took place but this was due to running-in and would have ceased after a short time once the asperities were flattened. It was accidentally discovered that pre-oxidation of the coated 316L steels, via vacuum heat treatment, resulted in an important and *major* improvement in corrosion-wear resistance.

1. Introduction

Although widely deployed in the general and specialist engineering sectors where good corrosion resistance is required [1], austenitic stainless steels are prone to galling and seizure in sliding contact situations; furthermore, they display poor resistance to wear and corrosion-wear. Surface engineering can provide a solution to this problem. Of the various possibilities, the application of thin hard coatings via the PVD technology of magnetron sputtering is attractive, provided contact pressures remain below the yield strength of the substrate (during use). To date, most research on the development of new material surfaces for corrosion-wear applications has centred on either *interstitial compound* coating materials like CrN or on S-phase (a nitrogen or carbon supersaturated stainless steel) that can either be applied as a monolithic coating via PVD [2,3] or via a diffusion treatment like low temperature ($<500\,^{\circ}C$) plasma or gaseous nitriding or carburizing [4–6]. It is notable, however, that relatively little attention has been placed on investigating *intermetallic* (substitutional) compound coatings. This research gap provided the impetus for the work reported here.

There are many types and compositions of intermetallic compound. Of these, coating compositions capable of producing FeCrNi σ-phase were selected for the present work. Since its discovery in monolithic steel structures by Bain and Griffiths [7], σ-phase was regarded as something to avoid, on account of its embrittling character on bulk properties. While, σ-phase is known to be hard (~940HV) its effect on corrosion behaviour is less clear. In one reported case [8] the general aqueous corrosion resistance of duplex stainless steel was seen to be unaffected by the phase while localised corrosion resistance was impaired. In another study [9] σ-phase was found to improve the corrosive-wear behaviour of stainless steels. The work reported here demonstrates the feasibility of using unbalanced magnetron sputter deposition for synthesising coatings based on the Fe–Cr–Ni ternary system with compositions suitable for the formation of σ-phase. The coatings, coded B1 and B2 (Fig. 1), were applied to AISI 316L substrates and subsequently characterized using a range of test procedures. Particular emphasis was given to investigating their corrosion-wear (CW) behaviour when subjected to reciprocation sliding contact with an apposing aluminium oxide (Al_2O_3) ball whilst immersed in physiological saline solution at 37 °C. A chance discovery demonstrated that the use of an additional process step, that of pre-oxidizing the coated 316L test-pieces in partial vacuum at 700 °C, caused a major improvement in corrosion-wear resistance.

2. Experimental

2.1. Uncoated 316L test pieces and substrates

The uncoated test pieces and the substrates were made from AISI 316L austenitic stainless steel with the composition and

* Corresponding author. Fax: +44 2380 593016.
E-mail address: peter_dearnley@talktalk.net (P.A. Dearnley).

0043-1648/$ - see front matter © 2012 Elsevier B.V. All rights reserved.
http://dx.doi.org/10.1016/j.wear.2012.09.002

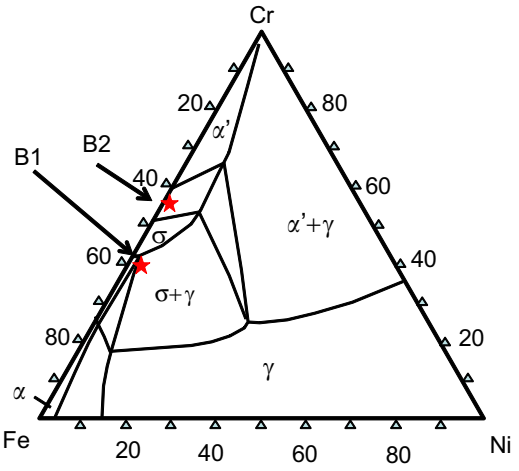

Fig. 1. Fe–Cr–Ni ternary isothermal section at 650 °C, showing the compositional position of coating materials B1 and B2 created in this study via magnetron sputter deposition. Axes are in weight %. Adapted from an original diagram in ASM Handbook, Alloy Phase Diagrams, vol. 3, 3rd printing, 1999, p. 3.44.

Table 1
AISI 316L substrate composition and microhardness.

Element	Fe	Cr	Mo	Ni	Si	Mn	C	S	P	HV0.1
Wt%	Bal.	17	2.3	12	0.03	2	0.03	0.03	0.04	231

micro-hardness shown in Table 1. Test discs, ~24 mm in diameter and 10 mm thick, were prepared by parting them off from a 24mm diameter AISI 316L austenitic stainless steel bar. The test faces of the discs were ground and polished, using SiC grinding and diamond lapping procedures respectively, to achieve a surface finish with an R_a better than 0.01 μm. The stainless steel contained small levels of sulphur (0.03 wt-%) that light optical microscopy revealed to be distributed as a small volume fraction of MnS inclusions.

2.2. Sputter deposition of Fe–Cr–Ni coatings

A closed-field unbalanced magnetron deposition facility was used to co-deposit the coatings, a facility that has been described in more detail in a previous publication [10]. The unbalanced configuration produces a closed magnetic field that confines the plasma between the opposing cathodes and enhances effective substrate ion bombardment during coating deposition. All substrates were rotated at 4 rpm during coating deposition which served to promote the formation of dense and uniformly thick coatings. The preferred procedure was to co-sputter using 99.5% purity Cr and AISI 304L (Fe–19Cr–10Ni) austenitic stainless steel targets. This arrangement yielded coatings of a composition suitable for σ-phase formation, designated B1 and B2 (Fig. 1). The actual coating compositions, determined using EDX (energy dispersive X-ray analysis) facilities attached to the SEMs described in Section 2.4, are cited in Table 2.

2.3. Heat treatment

In order to produce coatings containing crystalline σ-phase, several coated AISI 316L test-pieces were heated in vacuum ($\sim 10^{-4}$ Pa) to 700 °C for 2 and 10 h using a Carbolite vacuum tube furnace. After these durations, the test-pieces were transferred to a cold zone (by means of a special vacuum feed-through mechanism, without breaking the vacuum) and allowed to cool to room temperature. During the vacuum heat treatment of two batches of B1 and B2 coated 316L test-pieces at 700 °C for 10 h, a small leak of air took place, such that the pressure rose from $\sim 10^{-4}$ to $\sim 10^{-2}$ Pa. This resulted in these particular test-pieces becoming partially oxidized on their surfaces. Out of curiosity, it was decided to include these materials within the corrosion-wear testing plan, since prior work by Stack et al. [11,12], has shown that the pre-oxidation of metal surfaces can improve erosion-corrosion resistance of certain Fe and Ni based alloys.

Table 2
Coating composition (determined by EDX) and thickness.

Coating	Composition (wt%)			Thickness
	Cr	Fe	Ni	(μm)
B1	39.8	55.8	4.6	3.0
B2	55.4	42.0	2.6	2.3

2.4. Basic characterisation of coatings

Coating thickness and surface roughness were determined with the aid of a 2-D Form contacting Talysurf-120L profilometer set with a Gaussian cut-off filter of 0.8mm and a bandwidth of 100:1. Surface roughness parameters (R_a and R_q) were measured in two perpendicular directions. To determine coating thickness, surface regions were locally masked during deposition and then subsequently stripped to reveal a step. The height of each step (corresponding to the coating thickness) was then determined by profilometry. Coating thickness data is collated in Table 2. Coating topography was also imaged directly using a combination of light optical microscopy (LOM—Leica) and scanning electron microscopy (SEM). The latter comprised a high resolution Hitachi S-4100 field emission gun scanning electron microscope (FEG-SEM), a LEO-1530 FEG-SEM and an XL-30 Philips SEM. X-ray diffraction (XRD) was performed using Cu-K_α radiation under conventional Bragg-Brentano geometry (Bruker D8 and Siemens D500 diffractometers). Body centred cubic (bcc) crystal structures were identified. This was confirmed by determining the ratios of the $\sin^2\theta$ reflections and comparing these with known quadratic forms of the Miller indices of this structure [13] while any σ-phase was identified by comparing the obtained d-spacing data (corrected for systematic errors) by reference to the ICDD powder diffraction file no. 3-065-6712 (corresponding to the FeCr σ-phase, with unit cell dimensions of $a=b=0.87966$ nm; $c=0.45582$ nm and $\alpha=\gamma=\beta=90^\circ$).

Knoop (HK) and Vickers (HV) microhardness values were obtained using a Shimadzu HMV 2000 microhardness tester. Measurements were repeated five times. Nanohardness, the elastic modulus and elastic recovery parameter were obtained by using a Nano Test instrument (Micromaterials, Wrexham, UK) equipped with a diamond Berkovich indenter. Depth versus load hysteresis tests were conducted using the depth controlled mode of the instrument which was set to 200 nm. The loading and unloading was applied at 3 mN/s with a dwell period of 30 s under maximum load. This allowed the indenter to settle before unloading. The nano-indentation tests were repeated 20 times and the raw data subsequently reviewed to eliminate anomalous data. No hardness data was determined for the pre-oxidised test-pieces.

2.5. Corrosion-wear experiments

Simple configuration pin-on-plate reciprocating corrosion-wear tests were performed using a sliding frequency of 1 Hz with a stroke length of 8mm in a 0.89% NaCl (physiological saline) solution maintained at 37 °C (by an external isothermal water supply).

Further details of the apparatus used here are reported elsewhere [14]. A 7.96 mm diameter sintered Al_2O_3 ball bearing was used as the counterface test surface to avoid adverse galvanic coupling corrosion reactions with the metallic (coated and uncoated 316L) test plates. The test mass used, 100 g, equating to a normal force of 0.98 N, gave a maximum Hertzian compressive pressure of 525 MPa that resulted in a maximum *subsurface* shear stress (τ) of ~163 MPa (~43% of the shear yield strength τ_y of 316L, which was ~377 MPa). The latter value was estimated from its hardness, i.e., $\tau_y \sim H/6$, which Hertz contact mechanics calculations showed to act at 11 μm beneath the surface. Hence, the subsurface was not predicted to plastically deform beneath the coatings during the sliding contact test (from the resolved normal force acting through the Al_2O_3 ball).

After corrosion-wear testing a groove or track was produced in the coated and uncoated test plates.

The amount of surface material removed (the total area material loss—TML) as a result of the sliding contact tests was estimated from the corrosion-wear track (scar) cross-section. This parameter was determined from 2-D contacting surface profilometry (Talysurf) traces, obtained at three different positions along the track length. Their mean value and the standard deviations about the mean were then determined. In addition, 3-D non-contacting white light optical profilometry (Wyko-Veeco) was used to image and quantify the roughness of the corrosion-wear tracks and the worn Al_2O_3 ball counterfaces.

Corrosion-wear tests were carried out under three different electrochemical conditions: 1. OCP (open circuit potential); 2 PS (potentiostatic) at +50 mV Ag/AgCl (the potential relative to a standard Ag/AgCl test cell) and; 3. CP (cathodic protection) at −1000 mV versus Ag/AgCl conditions. All tests were repeated twice and a high reproducibility was observed. The PS value of 50 mV was chosen because preliminary static (without sliding) tests on uncoated AISI 316L showed that larger, potentials of 200 mV or greater caused the passive layer to break down spontaneously, particularly at defects like small MnS inclusions, while other tests carried out at 100 and 150 mV, were unsuitable due to very high corrosion currents being observed after an initial 'incubation time' of several minutes. Such breakdowns did not take place for tests carried out at 50 mV for either the coated or uncoated 316L test materials. The purpose of PS testing was to stimulate conditions where anodic corrosion made a major antagonistic (synergistic) contribution to the total area material loss (TML_{PS}) via the mechanical disruption of the passive film by the Al_2O_3 ball slider, whereas, the purpose of the CP tests was to suppress anodic corrosion enabling the total area material loss to be determined under the action of mechanical wear processes alone (TML_{CP}).

2.6. Corrosion-wear analysis

The total material loss (TML) due to corrosion-wear can be defined as [3,15,16]

$$TML = C + M + A \quad (1)$$

where C and M are the surface material losses due to corrosion (chemical wear or ion solution) and mechanical wear (particle loss) respectively and A is the sum of the synergistic or more precisely, the ***antagonistic***, components of material loss i.e.,

$$A = M_C + C_M \quad (2)$$

where M_C is the mechanical wear loss antagonized by corrosion action and C_M is the corrosion (chemical wear/ion solution) rate antagonized by mechanical action. The former process is manifest in the longer term and is essentially a sequential process of corrosion pitting and coating blistering followed by mechanical break-down and material loss through the removal of micro-fragments. In the context of the corrosion-wear of coated stainless steels this has previously been termed Type II CW (corrosion-wear) [3,16]. In contrast, C_M is a continuous, rather than a sequential, process. It is a process whereby a passive film is formed in-situ that is repeatedly broken down and replaced during repetitive sliding contact. The latter process had been called Type I CW (corrosion-wear [3,16], and is depicted schematically in Fig. 2. Hence, we can re-write Eq. (2) as:

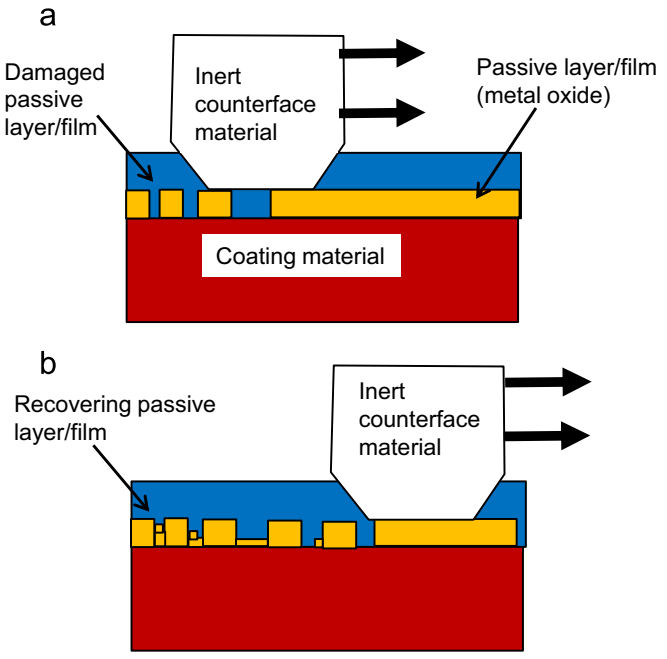

Fig. 2. Schematic depiction of Type I antagonistic corrosion-wear loss. After Dearnley and Aldrich-Smith [3].

$$A = \text{Type I CW} + \text{Type II CW} \quad (3)$$

In the present work, Type II CW was never observed for the durations used in the reciprocation sliding tests (60 min). Accordingly, M_C in Eq. (2) can be assumed to be zero. Similarly, ion solution from general corrosion, outside the sliding contact region was minimal. This can be gleaned from the output corrosion-currents measured before and after the onset of sliding contact, during potentiostatic testing (+50 mV Ag/AgCl). An example is shown on Fig. 3, which reveals the corrosion current to be very small (< 0.5 μA) during these stages, since the passive film was undisturbed. However, at the onset of sliding the corrosion current increased significantly (to ~30 μA) due to disruption of the film in this example (Fig. 3) and the triggering of Type I corrosion-wear. [An identical effect would have taken place under OCP conditions as was inferred from the fall in OCP from initial values in the range of 12.5 to 30 mV (versus Ag/AgCl) when the passive film was intact to −125 to −330 mV (Fig. 3**b**) produced upon application of the sliding Al_2O_3 ball which ruptured the film.] Accordingly the term C in Eq. (1), the background ion solution, can be considered to be practically zero for the tests conducted here.

The CP tests (mentioned above) suppressed anodic dissolution. Hence, the total area material loss determined under these conditions (TML_{CP}) can be assumed to be that due the mechanical wear loss alone (M in Eq. (1)). In the present work, we have attributed this type of degradation to be principally due to micro-asperity shearing or superficial plastic deformation and fracture, as depicted schematically in Fig. 4. It eventuated, however, that

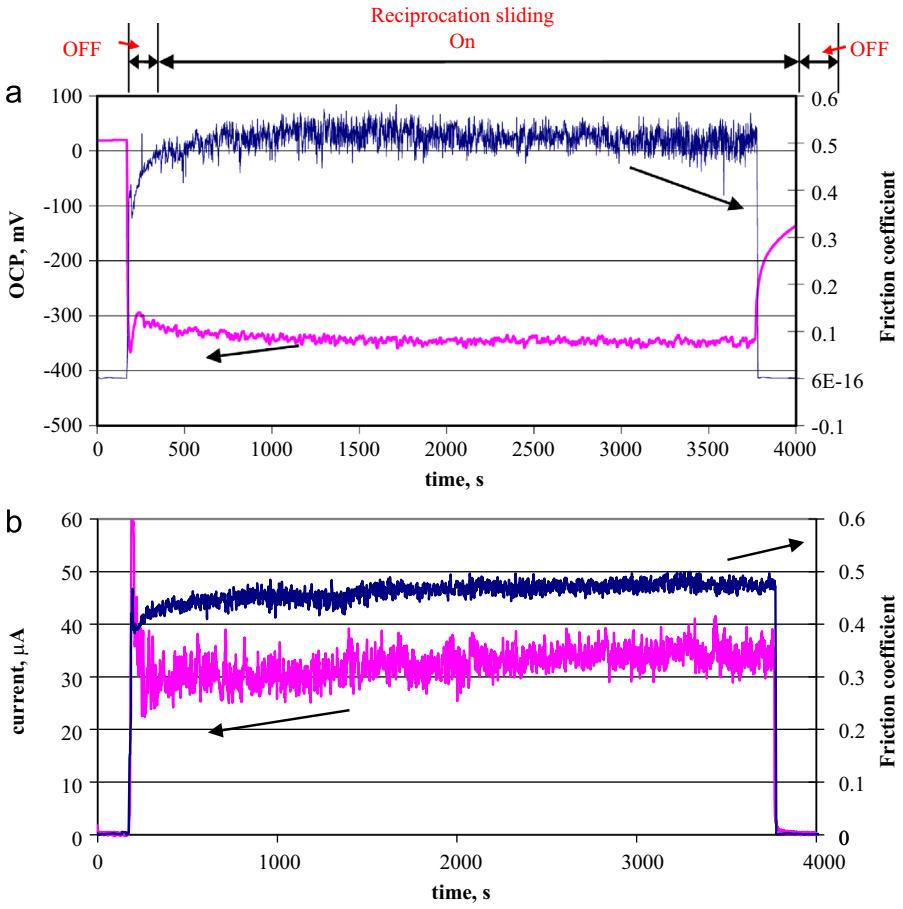

Fig. 3. Examples of data outputs from corrosion-wear test cell, for Al_2O_3 pin (6 mm dia ball) sliding against uncoated 316L immersed in 0.9% NaCl at 37 °C: (a) under open circuit potential conditions and; (b) potentiostatic conditions , 50.0 mV versus Ag/AgCl. Note the rapid changes in OCP and anodic current at the onset of testing, due to disruption of the passive film.

for the test conditions used here, this effect was only manifest during running-in of the test surfaces.

By re-writing Eqs. (2) and (3) as:-

$$A \approx C_M = \text{Type I CW} \tag{4}$$

$$TML \approx M + C_M \approx TML_{CP} + C_M \tag{5}$$

Specifically for open circuit conditions:

$$TML_{OCP} \approx M + C_M \approx TML_{CP} + C_M \tag{6}$$

Since TML_{OCP} and TML_{CP} can be obtained from experiment, it is possible to find C_M viz:

$$C_M \approx TML_{OCP} - TML_{CP} \approx A \approx \text{Type I CW} \tag{7}$$

Further, the proportion of TML_{OCP} due to Type I CW can be obtained from the ratio:

$$C_M / TML_{OCP} \tag{8}$$

which is a direct measure of the predominance (or not) of Type I CW.

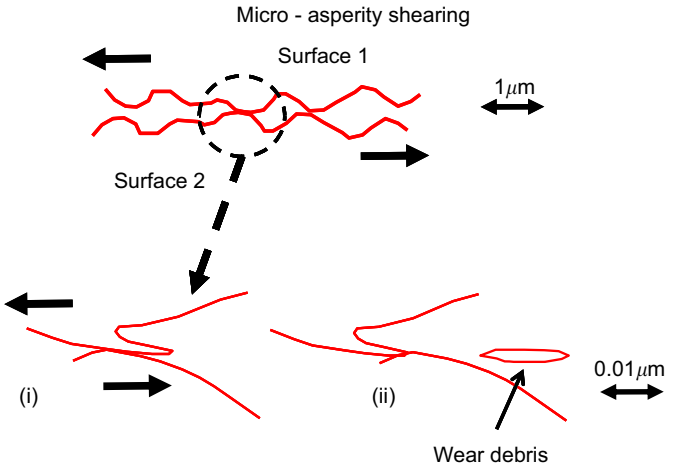

Fig. 4. Schematic depiction of mechanical wear loss via micro-asperity shearing/ superficial plastic deformation.

3. Results

3.1. Basic characterization of coated 316L.

The as-deposited B1 and B2 coatings had the compositions shown in Table 2 and their compositional positions on the Fe–Ni–Cr ternary equilibrium isothermal section at 650 °C are shown in Fig. 1.

FEGSEM observations of polished coating cross sections revealed all the coatings discussed here to be fully dense [10]. The composition of B1 (Table 2) places it near the triple point of the σ-FeCr, σ-FeCr+γFe(Cr) and αFe(Cr)+γFe(Cr) +σ-FeCr phase fields when formed under equilibrium conditions, whereas that of B2 (Table 2) would be within the Cr rich α′Cr(Fe) +σ-FeCr phase field, Fig. 1. Typical XRD spectra for the coated 316L test-pieces, in the as-received and vacuum heat treated states, are given in Fig. 5. The as-deposited B1 and B2 coatings were body centred cubic (BCC) solid solutions (designated α-Fe(Cr) and α′-Cr(Fe), respectively) that displayed strong

{1 1 0} fibre textures (Fig. 5). α-Fe(Cr) is α-Fe (ferrite) supersaturated with Cr, whilst α′-Cr(Fe) is α′-Cr supersaturated with Fe. Following, vacuum heat treatment at 700 °C for 2 and 10 h both phases decomposed forming various quantities and orientations of σ-FeCrNi (sigma phase). For the heat treated B1 coatings (designated B1HT2 and B1 HT10) the as-deposited α-Fe(Cr) was completely decomposed to σ-FeCr with a (0 0 2) preferred orientation. On the other hand, the B2 coated samples heat treated at 700 °C for 2 h (B2HT2) were only partly transformed to σ-FeCr (showing weak reflections (peaks) for σ-3 1 1, 0 0 2, 4 1 0, 3 3 0, 2 1 2, 4 1 1 and 3 3 1) and a residual {1 1 0} α′-Cr(Fe) peak. The latter peak remained in the sample heat treated for 10 h whilst the all the sigma phase reflections were strengthened, showing that further decomposition of the as deposited α-Fe(Cr) had taken place during the longer annealing treatment. The crystal structure of sigma phase is a complex body centred tetragonal (BCT), with 30 atoms per unit cell [7], compared to 2 atoms per unit cell for standard BCC or BCT structures.

Rockwell C indentation scratch testing results, reported previously [10], showed most coatings to be highly adherent, to their 316L substrates. Under the extreme contact pressure conditions of scratch testing, the substrates became plastically deformed, without causing spallation (flaking) of the coatings. The as deposited B1 and B2 coatings deformed without fracture (accommodating the deformation of the substrate), whilst the heat treated σ-FeCr coated test-pieces contained numerous randomly oriented micro-cracks in their deformed coatings, demonstrating their brittle character. This agrees with more general observations of σ-FeCr phase found in the microstructures of some stainless steels, which is associated with detrimental embrittlement [7].

Vickers (HV) and Knoop (HK) microhardness results for the uncoated and coated 316L test-pieces are given in Fig. 6, whilst nano-indentation hardness and reduced moduli data are given in Fig. 7. The indentation depth in the latter tests were fixed at 200 nm, whilst much deeper penetration (~1.5 μm) took place during Knoop indentation causing a lowering of the apparent hardness due to the influence of the softer substrate material (the coatings were only 3 μm thick, Table 2). To avoid any influence from the substrate the indentation depth should ideally be < 10% of the coating thickness. The nanoindentation hardness method demonstrated that significant hardening of the coating was brought about by the transformation of the α-Fe(Cr) or α′-Cr(Fe) phases to σ-FeCr during vacuum heat treatment, Fig. 7. Since the

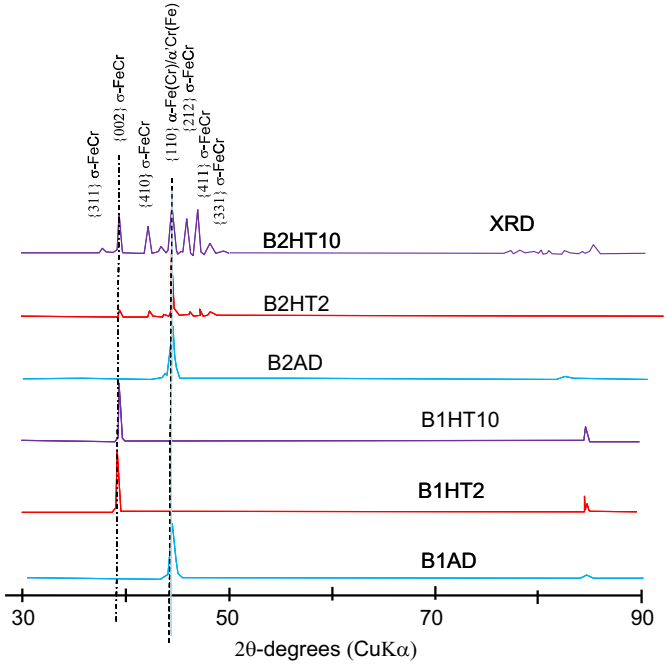

Fig. 5. XRD spectra of B1 and B2 coated 316L, in as-deposited and vacuum heat treated conditions. The vertical axis represents the counted number of X-ray photons.

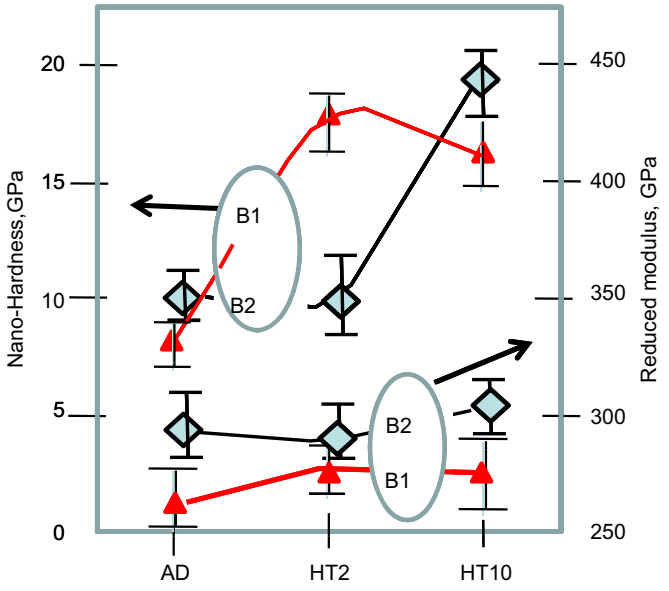

Fig. 7. *Nanoindentation* hardness and modulus of B1 and B2 coated 316L in as-deposited (AD) and vacuum annealed (HT2 and HT10) conditions. Error bars represent 1σ.

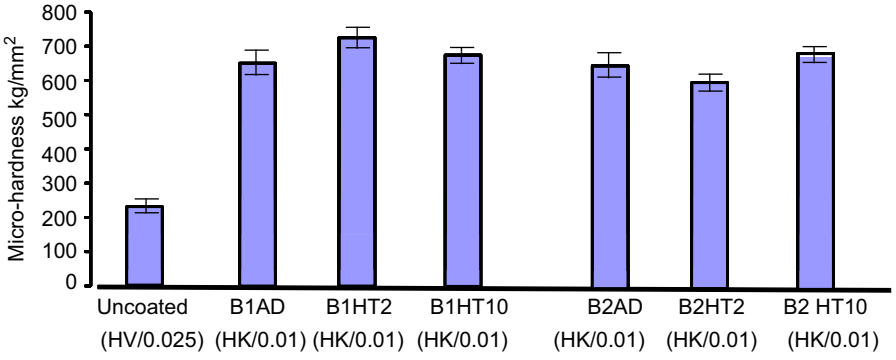

Fig. 6. Vickers (HV) and Knoop (HK) *micro*-hardness of B1 and B2 coated 316L in as-deposited and vacuum annealed conditions. Error bars represent 1σ.

conversion to σ-FeCr was incomplete for the B2 coating after 2 h annealing, it was only after 10hrs that a significant increase in hardness to > 15GPa was observed (Fig. 7).

3.2. Corrosion-wear tests

The total area material losses (TMLs) determined from profilometry, after corrosion-wear testing under open circuit potential (OCP) and potentiostatic (PS) conditions, are summarized in Fig. 8. These show most coated 316L variants to be only better than uncoated 316L test-pieces when tested under PS conditions.

Typical outputs from the instrumented corrosion-wear test cell, for an Al_2O_3 ball sliding against an uncoated 316L, under open circuit potential (OCP) and potentiostatic (PS) conditions are shown in Fig. 3. It can be seen that a large change in OCP and the anodic corrosion current (PS) takes place on the onset of sliding contact. This indicates a marked disruption to the passive film, a phenomenon that leads to the dissolution of the unprotected metallic surface beneath, via Type I corrosion-wear (Fig. 2). An identical type of behaviour was observed for both as received and heat treated coated 316L test-pieces. For convenience of presentation the *ranges* of anodic currents recorded during PS testing on all coated and uncoated test pieces have been

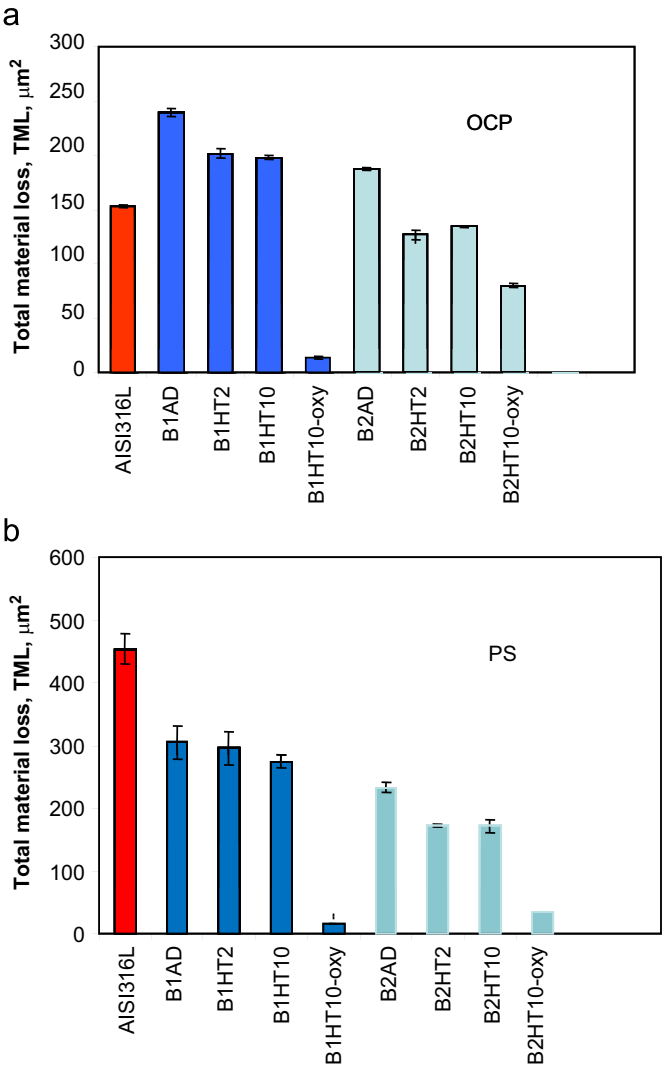

Fig. 8. Total area material loss, TML, (determined from corrosion-wear track areas) after testing under: (a) open circuit potential (OCP) and; (b) potentiostatic—PS (50 mV versus Ag/AgCl) testing of coated and uncoated 316L while immersed in 0.9% NaCl solution at 37 °C during sliding contact with an Al2O3 ball. Error bars represent 1σ.

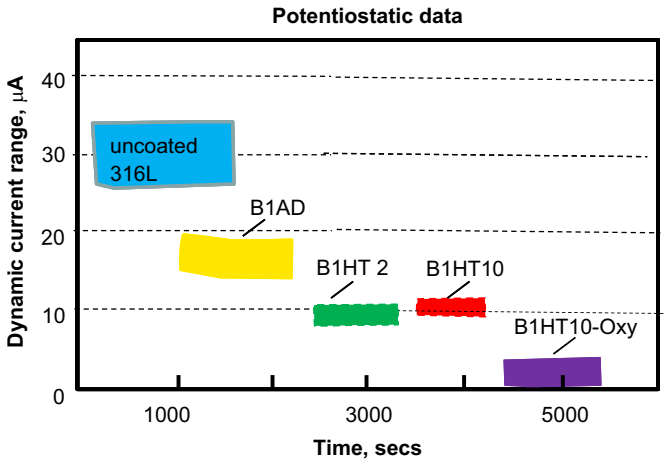

Fig. 9. Examples of collated steady-state anodic corrosion currents monitored during potentiostatic (50 mV versus Ag/AgCl) testing of coated and uncoated 316L while immersed in 0.9% NaCl solution at 37 °C during sliding contact with an Al_2O_3 ball.

collated together in one diagram, Fig. 9. These show that lower corrosion currents were produced by the sigma phase coated 316L compared to the as deposited α-Fe(Cr) coated and uncoated 316L test-pieces.

Evidence of *both* micro-asperity shearing *and* dynamic anodic dissolution was observed on many corrosion-wear tracks, indicating the regular co-existence of two mechanisms of surface degradation. A characteristic of dynamic anodic dissolution is the formation of smooth wear surfaces [3,14]; here material is removed progressively from the sliding contact surfaces via atomic diffusion. Figs. 10–13 show that the corrosion-wear surfaces become progressively smoother in the sequence uncoated 316L→ α-Fe(Cr) coated 316L (as deposited) →σ-FeCr coated (heat treated) 316L. The banding appearance, in the direction of reciprocation sliding (Figs. 10 and 11), is indicative of micro-asperity plastic shearing of the surfaces as depicted schematically in Fig. 4. This is shown in more detail in the FEGSEM image in Fig. 14. However, fewer shear bands were evident on the sigma phase containing coatings, Figs. 12 and 13.

3.3. Pre-oxidized test-pieces

These materials demonstrated a remarkable improvement in corrosion-wear resistance compared to the other coated and uncoated 316L, under both OCP and PS conditions, Fig. 8. The shallowness and narrowness of the resulting corrosion-wear tracks were evident in the light intensity mode of the Wyko optical profilometer, Fig. 15. Dynamic friction coefficients, measured during reciprocation sliding in the 0.9% NaCl solution, showed the B1HT10-oxy samples in particular to demonstrate a slightly lower value, compared to the non-oxidized test-pieces (Fig. 16).

3.4. Al_2O_3 ball surfaces

Examination of all the Al_2O_3 ball contact surfaces after corrosion-wear testing revealed them to be smoothly worn flats with no evidence of grain pull-out—a phenomenon previously reported for testing against Ti alloys [14,17]. Further, there was little evidence of material transfer from the coated and uncoated 316L test-pieces to the ball, [18].

3.5. Tests conducted under cathodic protection (CP) conditions.

As a first approximation, the area material loss under CP conditions, is that due to mechanical action alone. By subtracting

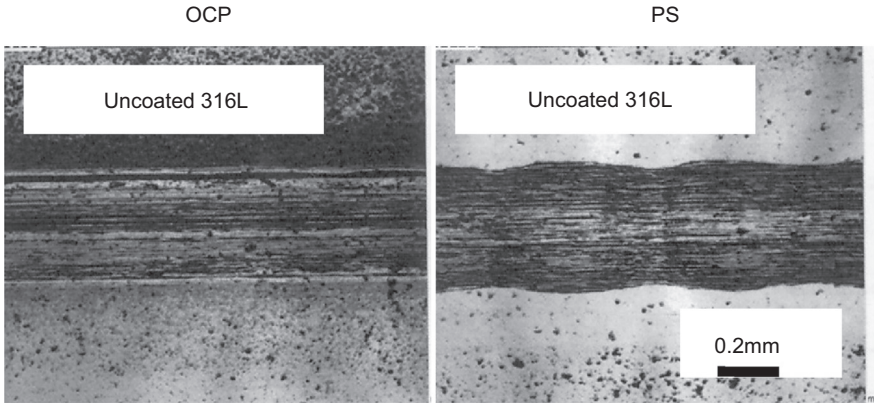

Fig. 10. Light intensity images (Wyko profilometer) of uncoated 316L corrosion-wear tracks produced under OCP (left) and PS (right) conditions after 3600 s of testing. Note banding of the tracks due to superficial plastic deformation in shear.

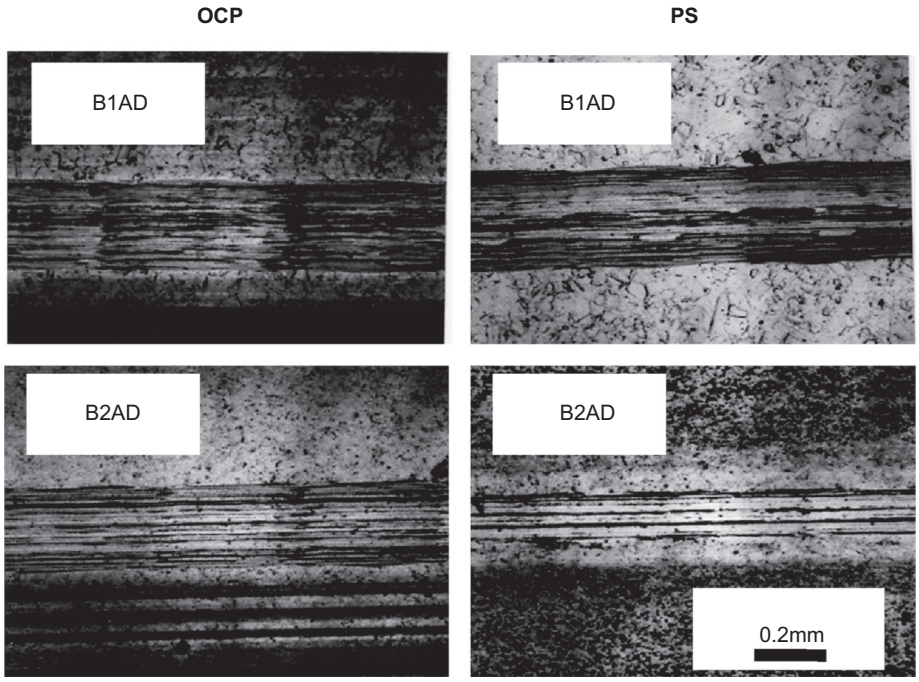

Fig. 11. Light intensity images (Wyko profilometer) of B1AD and B2AD (as-deposited) coated 316L corrosion-wear tracks produced under OCP (left) and PS (right) conditions after 3600 s of testing. Note banding of the tracks due to superficial plastic deformation in shear.

the area material loss under CP conditions from the area material loss under open circuit conditions, an estimate of the area material loss due to Type 1 corrosion-wear behaviour was determined (Eq (7)). Table 3 shows the estimated "chemical" area material loss values and the estimated chemical/mechanical material loss ratios (Eq. (8)). The latter ranged from 0.82 to 0.93 for all the coated and uncoated 316L test-pieces, indicating that the chemical driven wear processes was the dominant material loss process under open circuit potential (OCP) conditions and that ALL the estimated material loss ratios were *very similar*.

4. Discussion

4.1. The role of electrode potential on TML (total area material loss)

The purpose of PS testing at 50 mV was to stimulate mechanically antagonized corrosion (anodic dissolution), also termed Type I corrosion-wear (Fig. 2), and to be able to monitor the resulting corrosion currents, which was not possible under OCP conditions. Fig. 17 shows that there was a very good correlation between the total area material loss (TML_{PS}) and the measured anodic current for all tests made under PS conditions. The highest corrosion currents were recorded for the uncoated 316L and the lowest for the pre-oxidized B1 and B2 test-pieces, intermediate values being observed for the B1 and B2 coated cohorts.

The effect of Cr content of the test material surface on TML_{PS} and TML_{OCP} is shown in Fig. 18a while the influence of hardness on both TMLs is shown in Fig. 18b. It is apparent that Cr has a moderately strong effect on TML under PS conditions, with hardly any effect under OCP conditions, where the electrode potential was typically around −300 mV. In real applications the true value of OCP will depend upon the surrounding environment, especially the size of the anodic contact area with respect to any adjacent cathodic areas. For better transferability to other application environments it is useful to look at the overall influence of electrode potential on TML of the test material. This global view is shown in Fig. 19a and b for the B1 and B2 coated cohorts, respectively. Whilst a least squares linear regression fit was obtained for both sets of coated data, an exponential function

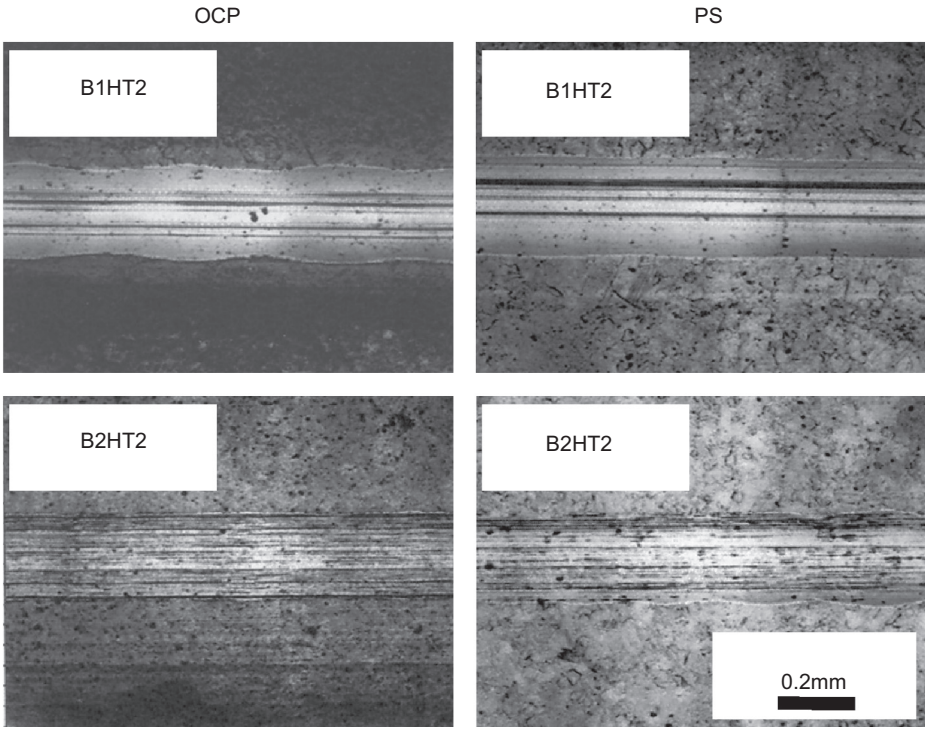

Fig. 12. Light intensity images (Wyko profilometer) of B1HT2 and B2HT2 (vacuum heat treated at 700 °C for 2 h) coated 316L corrosion-wear tracks produced under OCP (left) and PS (right) conditions after 3600 s of testing. Note banding of the tracks due to superficial plastic deformation in shear (lower two images).

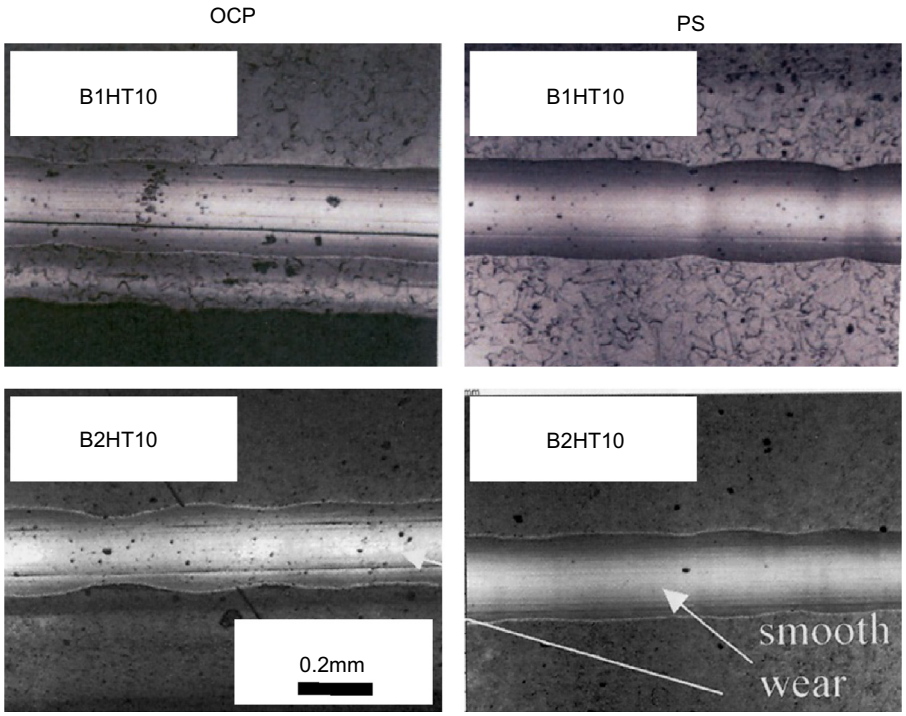

Fig. 13. Light intensity images (Wyko profilometer) of B1HT10 and B2HT10 (vacuum heat treated at 700 °C for 10 h) coated 316L corrosion-wear tracks produced under OCP (left) and PS (right) conditions after 3600 s of testing.

(obtained from the standard Microsoft Office Excel 2007 fitting routine) was found to provide a better fit for the uncoated 316L data, which takes into account the near three-fold increase in TML obtained when testing under an externally applied potential of 50 mV (versus Ag/AgCl). It is clear that this increase was electrochemically driven and that the relatively low hardness of the uncoated 316L had no effect on TML.

Fig. 19a and b demonstrates that the B1 coated cohorts were slightly more vulnerable to corrosive-wear (Type 1) than the B2 cohorts—the slope of the former curve being steeper than the latter. This is attributed to the higher Cr content of the B2 cohort (Table 2) compared to that of the B1 coatings. This indicates that Type B2 variant passive films were more strongly adherent (during Type 1 corrosion-wear, Fig. 2), than that formed on the B1 coatings,

regardless of whether they were solid solution based or σ-phase based (Fig. 5). The higher surface hardness of most of the σ-phase based coated 316 test-pieces (Fig. 7) was important only in reducing the amount of visible superficial plastic deformation (depicted schematically in Fig. 4) as indicated by the increasing absence of shear bands in the sequence uncoated 316L→B1AD & B2AD→B1HT & B2HT coated variants (respectively Fig. 10→Fig. 11→Fig. 12→Fig. 13). Calculations (Table 3) of the estimated chemical/mechanical material loss ratios (from Eq. (8)) gave values from 0.82 to 0.93, which supports the argument that superficial plastic deformation, whether visible or not, was never rate controlling and at best played a very minor part in the TML of all test materials under the conditions used here.

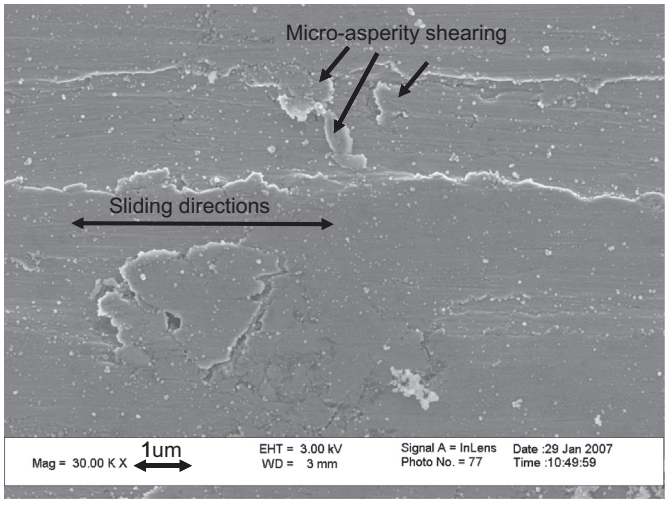

Fig. 14. FEGSEM image of uncoated 316L corrosion-wear track produced under PS conditions for 3600 s. Whilst there are many smooth areas, flattened/smeared asperities, indicative of micro-asperity shearing/superficial plastic deformation are visible. Double arrow indicates directions of reciprocation sliding.

It is of interest to consider an explanation for the higher value of TML observed for the non-oxidized coated 316L test pieces compared to the uncoated test pieces, under OCP conditions (where the electrode potential was approximately −300 mV for all samples), which was in strong contrast to the trend observed under PS conditions (50 mV), where the situation was reversed. To explain this effect unequivocally, further testing would be necessary to establish the complete anodic polarization behaviour of the test materials under sliding contact conditions. Since, it has been argued that the TML was almost entirely due to ion solution, the anodic polarization behaviour was probably of the character shown schematically in Fig. 20, which incorporate the results of Fig. 19. Here, it is proposed that tests conducted under OCP conditions, produced a slightly higher ion current and rate of solution for the non-oxidized coated cohorts compared to the uncoated 316L. It is further proposed that under PS conditions (50 mV), the test potential was beyond the breakdown potential (F_{bd}) of the passive film for the uncoated 316L (Fig. 20) whilst remaining below E_{bd} for the coated 316L test-pieces (Fig. 20). The hypothesis also suggests (under OCP conditions) that the passive film formed on the non-oxidised coatings was prone to a form of short term mechanical damage that aided ion diffusion through it, compared to the uncoated 316L passive film that was more impervious to ionic diffusion. Clearly deeper work is required to fully elucidate the true character of ionic diffusion through the passive films concerned under PS and OCP conditions.

4.2. The importance of pre-oxidation

Pre-oxidation of the coated 316L test-pieces proved a powerful method for enhancing resistance to mechanically antagonized corrosion (Type I Corrosion-wear) under open circuit potential and potentiostatic (+50 mV versus a Ag/AgCl reference electrode) conditions, Fig. 19. (The latter test condition caused a three-fold increase in the TML value for the uncoated 316L test-pieces.) The precise character of the pre-oxidized materials has yet to be investigated in depth. It is clear however that the oxide for these

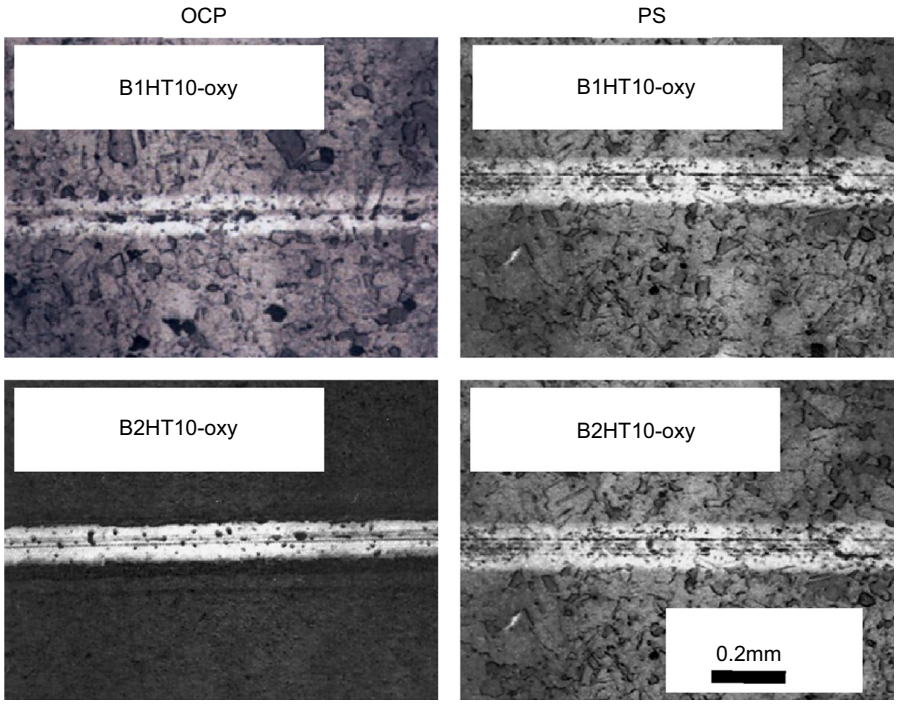

Fig. 15. Light intensity images (Wyko profilometer) of pre-oxidised B1HT10 and B2HT10 (vacuum heat treated at 700 °C for 10 h) coated 316L corrosion-wear tracks produced under OCP (left) and PS (right) conditions after 3600 s of testing.

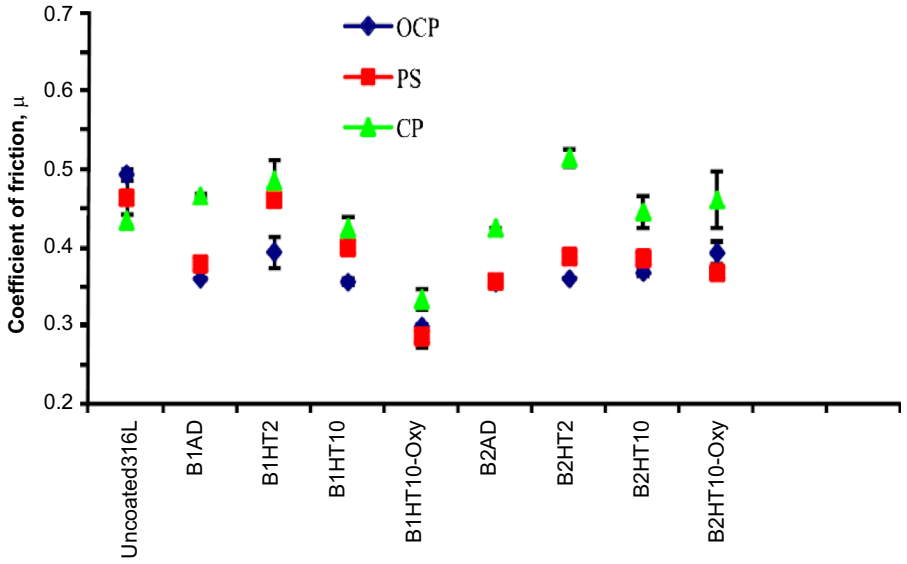

Fig. 16. Average dynamic friction coefficients measured during corrosion-wear testing under open circuit potential (OCP), potentiostatic (PS) [50 mV Ag/AgCl] and cathodic protection (CP) [−1.0 VAg/AgCl] testing of coated and uncoated 316L while immersed in 0.9% NaCl solution at 37 °C during sliding contact with an Al_2O_3 ball. Error bars represent 1σ.

Table 3
Corrosion-wear data.

Sample	OCP total area material loss (μm^2)	CP total area material loss (μm^2)	Mechanically antagonized corrosion (area) material loss (μm^2) Type I CW	Area material loss ratio
	TML_{OCP}	TML_{CP}	C_M	C_M/TML_{OCP}
U/C AISI 316L	153	11	142	0.93
B1AD	240	21	219	0.91
B1HT2	202	24	178	0.88
B1HT10	198	14	184	0.93
B2AD	184	24	160	0.87
B2HT2	124	22	102	0.82
B2HT10	132	12	120	0.91

materials must have been be very tenaciously adhered to the sigma phase coatings in comparison to the passive films formed in-situ on the uncoated and the non-pre-oxidized B1 and B2 coated 316L cohorts (during corrosion-wear testing). This finding is similar to that reported previously by Stack and co-workers [11,12] who investigated the effect of pre-oxidizing metallic alloys on their subsequent response to an erosion-corrosion test environment where surfaces were continually bombarded by micrometre sized silica particles suspended in an oxidizing fluidized bed atmosphere at elevated temperature. They [11,12] demonstrated that pre-oxidation was very effective in providing a highly adherent protective passive film, provided the pre-oxide was grown in a low partial pressure of moisture (H_2O)—the balance of the atmosphere being H_2. They also showed that when pre-oxidation was carried out in higher partial pressures of oxygen, poorly adhered oxide films resulted. They argue that pre-oxidation at low pressure is key; it enables passive films to grow more densely, albeit more slowly [11,12]. In the work presented here, pre-oxidation, was achieved accidently in partial vacuum of approximately 10^{-2} Pa. Using the same reasoning we argue that the resultant oxide layer was similarly very dense (due to it being formed over several hours at 700 °C) and accordingly very adherent and better suited to resisting mechanically antagonized corrosion, compared to the more rapidly forming passive film that formed in-situ (after a few seconds) on the uncoated and non-pre-oxidized coated 316L test pieces, during corrosion-wear testing.

4.3. The role of hardness (shear yield strength) on TML (total area material loss)

The friction coefficient (μ) for most tests was in the range of 0.3 to 0.5 (Fig. 16), which because a normal force (F_N) of 0.98 N (100 g) was applied during the corrosion-wear tests, equates the friction force (F_f) values in the range of 0.3 N to 0.5 N, respectively. From Hertz contact mechanics the elastic contact radius and contact area were calculated to be 2.736×10^{-2} mm and $\sim 2.35 \times 10^{-3}$ mm^2, respectively; this translates to a superficial surface shear stress in the range of 125 to 208 MPa during all of the corrosion-wear tests. The shear yield strength (τ_y) of the coated and uncoated surfaces can be estimated from their hardness, given that $\tau_y \sim H/6$ [19]. This analysis gives τ_y values ~378, ~1300 to 1600 and ~2600 to 3000 MPa for uncoated 316L, as-deposited B1 and B2 and the heat treated (HT series) σ-phase coated 316L variants, respectively. Hence, ALL the coatings and the uncoated 316L had sufficient yield strength to prevent superficial plastic deformation being a major factor contributor to the observed TML values. The observation of shear band formation (Figs. 10, 11 and 14) would appear to due to running-in when the surfaces were sufficiently uneven to cause localized plastic deformation at micro-asperities, i.e., when initial contact pressures at surface asperities exceeded the shear strength of the metallic surfaces. However, such deformation did not contribute significantly to the TML values summarized in Fig. 8.

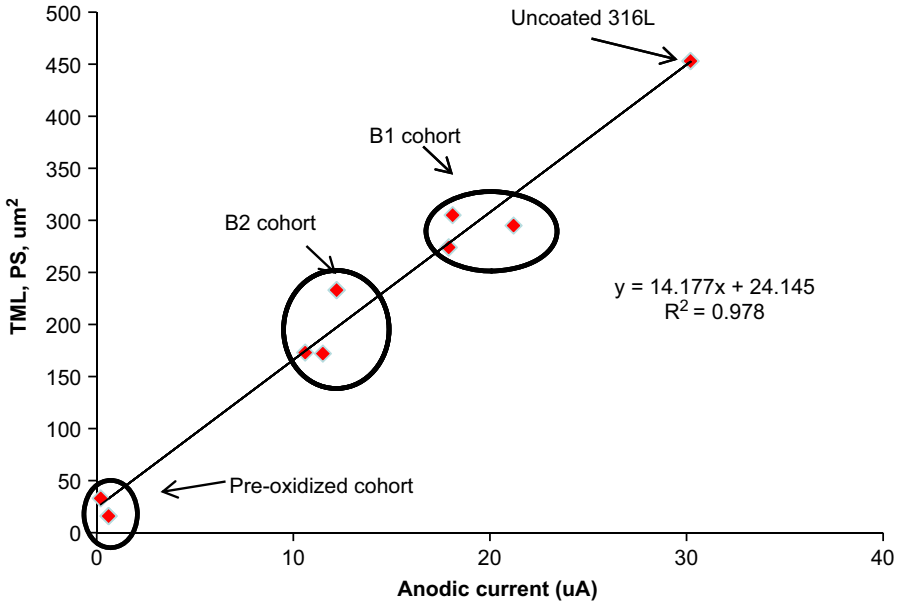

Fig. 17. Correlation between total area material loss (TML) and dynamic corrosion current for coated and uncoated 316L test pieces tested under potentiostatic (50 mV with respect to Ag/AgCl standard electrode) electrochemical conditions.

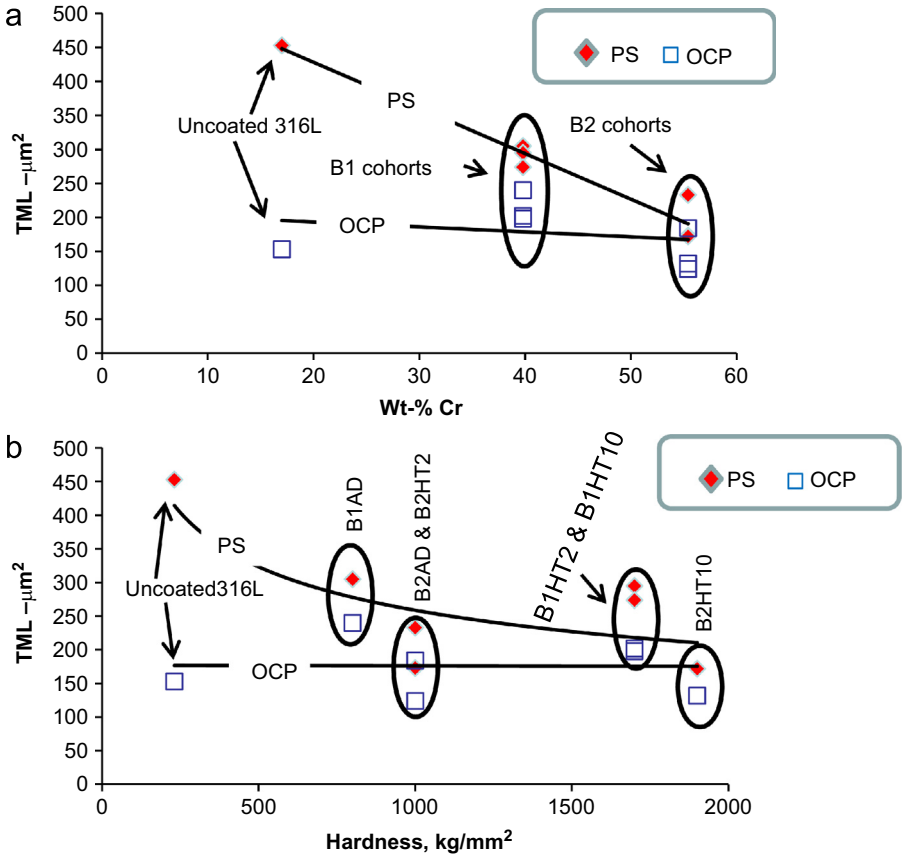

Fig. 18. Correlation between total area material loss (TML) and (a) wt%Cr content in the exposed uncoated and coated 316L test pieces; (b) hardness of the exposed uncoated and coated 316L test pieces;

5. Conclusions

A procedure was developed to apply a series of Cr-based hard coatings to polished austenitic stainless steel 316L using unbalanced magnetron sputter deposition. Two basic coating compositions (weight%) were produced: type B1 (Fe–38Cr–8Ni) and type B2 (Fe–55Cr–2.5Ni). Some of the coated AISI 316L test pieces were vacuum heat treated ($\sim 10^{-4}$ Pa) at 700 °C for 2 and 10 h to stimulate the formation of FeCrNi σ-phase, while a few others were accidentally pre-oxidized during vacuum heat treatment by leaking air into the chamber raising the total pressure to $\sim 10^{-2}$ Pa (at the same temperature). The following conclusions

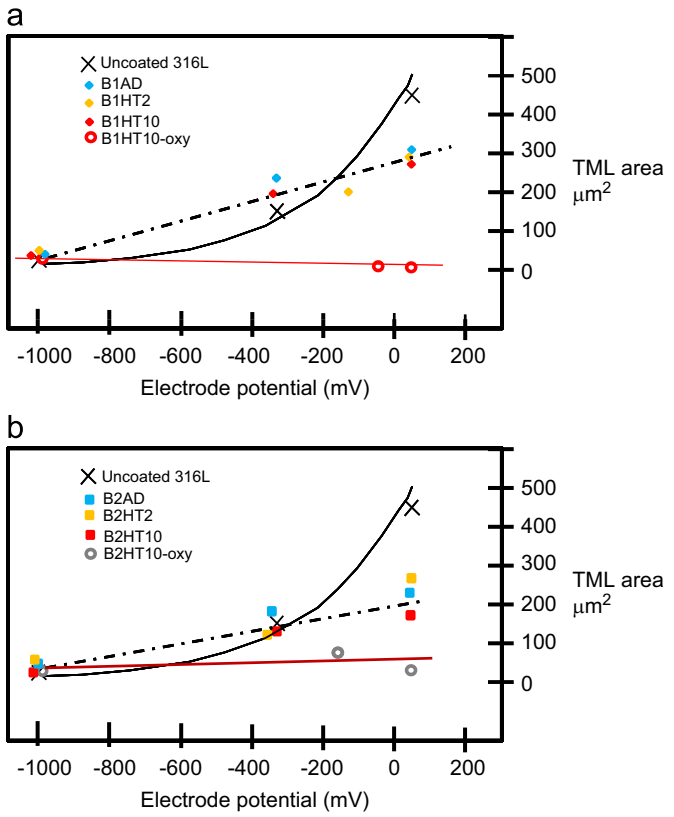

Fig. 19. Correlation between total area material loss (TML) and electrode potential with respect to Ag/AgCl standard electrode while immersed in 0.9% NaCl solution at 37 °C during sliding contact with an Al_2O_3 ball. Data for uncoated 316L is included in both graphs for ease of comparison. Some data points are off-set to aid clearer visibility. (a) B1 cohort and (a) B2 cohort.

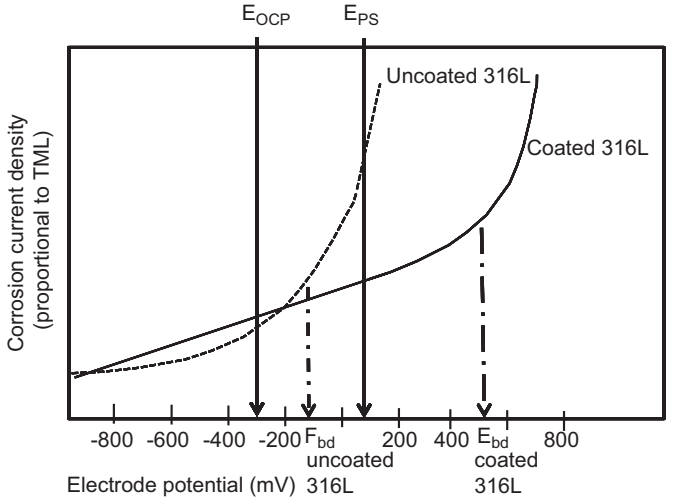

Fig. 20. Schematic current density versus electrode potential diagram during dynamic corrosion-wear of coated and uncoated 316L showing relative positions of OCP, PS testing conditions and hypothetical breakdown potentials (E_{bd}).

are based upon corrosion-wear testing of the coated and uncoated 316L test-pieces using an aluminium oxide ball (pin) to slide against their surfaces whilst immersed in 0.9% NaCl solution at 37 °C, under a normal force of ~1 N (100 g).

1. The total area material loss (TML) was dominated by mechanically antagonized corrosion (Type I corrosion-wear) when tests were conducted under OCP (in the order −300 mV) and PS (+50 mV) electrochemical conditions. Testing under PS conditions, further stimulated Type I corrosion-wear, which was supported by the finding that there was a strong linear correlation between the anodic corrosion current and the TML.
2. Observations and calculations indicated that dynamic anodic dissolution (via Type I corrosion-wear) was the rate determining mechanism of material loss, representing more than 80% of the TML, under open circuit potential conditions.
3. The total area material loss (TML) of the coated and uncoated 316L test-pieces was proportional to the electrode potential in the range of −1000 to +50 mV (relative to a standard Ag/AgCl electrode). A slightly greater tendency for anodic dissolution was shown by the B1 coated series/cohort compared to the B2 coated cohort. In the electrode potential range of −1000 to −300 mV the uncoated 316L showed similar TML behaviour to the coated variants whereas the pre-oxidized test-pieces, showed a near constant, and *very low*, TML values. At a higher electrode potential of +50 mV, a major (three fold) increase in the TML of uncoated 316L took place, whereas, under the same conditions, all coated variants displayed TML values that were only one third to a half of those for uncoated 316L.
4. Pre-oxidation of the heat treated B1 and B2 coated 316L test-pieces caused a major reduction in corrosion-wear. This was attributed to the pre-oxidized oxide film being exceptionally adherent and resistant to mechanical damage during sliding contact in comparison to the passive films formed in-situ (during corrosion-wear testing) on the other coated and uncoated test-material surfaces which were poorly adherent.
5. A minor contribution to the TML was caused through superficial plastic deformation (micro-asperity shearing) of the metallic contact surfaces due to running-in. Such material loss would have ceased once the asperities were flattened.
6. The effect of increasing the Cr content of the surface was to cause a significant reduction in TML under PS conditions, whilst the TML remained almost constant under OCP conditions.
7. A higher value of TML was observed for the non-oxidized coated 316L test pieces compared to the uncoated test pieces, under OCP conditions (where the electrode potential was approximately −300 mV for all samples), which was in strong contrast to the trend observed under PS conditions (50 mV), where the situation was reversed. A hypothesis was proposed that the passive film formed on the non-oxidised coatings (under OCP conditions) was more prone to short-term mechanical damage which aided ion diffusion through it, compared to the uncoated 316L passive film. It was further proposed that under PS conditions (50 mV), the test potential was above the breakdown potential (F_{bd}) of the passive film for the uncoated 316L (Fig. 20) causing a high rate of ion solution whereas the coated 316L test-pieces remained below their E_{bd} value and ion solution was moderate.

Acknowledgments

One author (BM) is indebted to The University of Malta for the provision of a research scholarship. Both authors thank Prof. Ing. Maurice Grech, former head of the Metallurgy & Materials Engineering Department (UM) for his enthusiastic personal support of this project. The technical advice of Dr Karl Dahm presently at Massey University, New Zealand, is gratefully acknowledged.

References

[1] D.A. Jones, second ed., Prentice Hall, New Jersey, 1996.
[2] K.L. Dahm, P.A. Dearnley, On the nature, properties and wear response of s-phase (nitrogen-alloyed stainless steel) coatings on AISI 316L, Proceedings of the Institution of Mechanical Engineers 214 (L4) (2000) 181–198.

[3] P.A. Dearnley, G. Aldrich-Smith, Corrosion-wear mechanisms of hard coated austenitic 316L stainless steels, Wear 256 (5) (2004) 491–499.
[4] RH. Van der Jegt, BH. Kolster, MWH. Gillham, Anti-wear/corrosion treatment of finished austenitic stainless steel components: the hardcor process, Materials and Design **12** (1) (1991) 41–46.
[5] Y. Sun, X. Li, T. Bell, Low temperature plasma carburising of austenitic stainless steels for improved wear and corrosion resistance, Surface Engineering **15** (1999) 49–54.
[6] Y. Sun, X. Li, T. Bell, Structural characteristics of low temperature plasma carburised austenitic stainless steel, Materials Science and Technology **15** (1999) 1171–1178.
[7] G. Krauss, Steels: Heat Treatment and Processing Principles, ASM International, 4th Printing, Materials Park, OH, 1995, p. 370.
[8] J.H. Potgieter, British Corrosion Journal 27 (1992) 219.
[9] X. Lu, S. Li, X. Jiang, Effects of σ-phase in stainless steels on corrosive wear behavior in sulfuric acid, Wear 251 (2001) 1234–1238.
[10] B. Mallia, K.L. Dahm, A. Ogwu, P.A. Dearnley, The structure & properties of magnetron sputtered Fe–Cr–Ni coatings containing sigma phase, Plasma Processes and Polymers **4** (2007) S113–S119.
[11] M.M. Stack, F.H. Stott, G.C. Wood, The effect of pre-oxidation of chromia and alumina forming alloys on erosion in laboratory simulated fluidized-bed conditions, Corrosion Science **33** (6) (1992) 965–983.
[12] M.M. Stack, F.H. Stott, G.C. Wood, Erosion–corrosion of pre-oxidized Incoloy 800H in fluidized bed environments, Materials Science & Technology **7** (1991) 1128–1137.
[13] Elements of X-ray Diffraction, B.D. Cullity, second ed., Addison-Wesley, London 1978.
[14] B. Mallia, P.A. Dearnley, The corrosion-wear response of Cr–Ti coatings, Wear 263 (2007) 679–690.
[15] S.W. Watson, F.J. Friedersdorf, B.W. Madsen, S.D. Cramer, Methods of measuring wear-corrosion synergism, Wear 181-183 (1995) 476–484.
[16] R.J.K. Wood, Tribo-corrosion of coatings: a review, Journal of Physics: D—Applied Physics 40 (18) (2007) 5502–5521.
[17] P.A. Dearnley, K.L Dahm, H. Çimenoğlu, The corrosion-wear behaviour of thermally oxidized CP–Ti and Ti–6Al–4V, Wear 256 (5) (2004) 469–479.
[18] B. Mallia, Novel Nanostructured Coatings for Extreme Tribological Environments, Ph.D. Thesis, University of Leeds, 2008.
[19] P.A. Dearnley, J. Gummersbach, H. Weiss, A.A. Ogwu, T.J. Davies, The sliding wear resistance and frictional characteristics of surface modified aluminium alloys under extreme pressure, Wear 225-229 (1999) 127–134.